Low-lying electronic states with giant linear dichroic ratio observed in PdSe₂
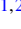
Chenyi Gu,[1,2] Xiaowei Liu,[3] Cheng Chen,[4,5,6] Aiji Liang,[4,5,6] Wei Guo ●,[1,2] Xinrui Yang,[1,2] Jian Zhou ●,[1,2] Chris Jozwiak,[6]
Aaron Bostwick,[6] Zhongkai Liu,[4,5] Shi-Jun Liang,[3] Yulin Chen,[4,5,7] Feng Miao,[3,*] Eli Rotenberg ●,[6] and Yuefeng Nie ●[1,2,†]

[1]*National Laboratory of Solid State Microstructures, Jiangsu Key Laboratory of Artificial Functional Materials,*
College of Engineering and Applied Sciences, Nanjing University, Nanjing 210093, China
[2]*Collaborative Innovation Center of Advanced Microstructures, Nanjing University, Nanjing 210093, China*
[3]*Institute of Brain-Inspired Intelligence, National Laboratory of Solid State Microstructures, School of Physics,*
Collaborative Innovation Center of Advanced Microstructures, Nanjing University, Nanjing 210093, China
[4]*School of Physical Science and Technology, ShanghaiTech University, Shanghai 201210, China*
[5]*ShanghaiTech Laboratory for Topological Physics, Shanghai 201210, China*
[6]*Advanced Light Source, Lawrence Berkeley National Laboratory, Berkeley, California 94720, USA*
[7]*Department of Physics, University of Oxford, Oxford OX1 3PU, United Kingdom*

Palladium diselenide (PdSe₂), a recently exploited transition metal dichalcogenide material with a thickness-dependent band gap, anisotropic optical response, and high air stability, has shown excellent performance in electronics and polarization photodetection. However, the origin of the intriguing optical response in this material from a perspective of electronic band structure, including the orbital character and the experimental demonstration of its indirect band gap, has not yet been explored. By applying polarization-dependent, angle-resolved photoemission spectroscopy and density functional theory calculations, we measured an indirect band gap of bulk PdSe₂ to be ∼0.36 eV. Moreover, the orbital-resolved electronic band structure reveals a top valence band dominated by Pd-$d_{3z^2-r^2}$ and Se-p_z orbitals, which gives rise to an unprecedented giant linear dichroic ratio of 10, showing a huge orbital-induced anisotropy. Our results elucidate the semiconducting nature of PdSe₂ and propose PdSe₂ to be an intrinsically orbital-engineered material with giant anisotropy for polarization-related optical applications.

Introduction. Polarization of light and its measurement are of great interest in various areas of science, including diffractive optics [1], nanophotonics [2], bionics [3], etc. Recently, anisotropic layered materials have demonstrated their great advantages in the design of polarization photodetectors [4–9] using their intrinsic optical anisotropy other than extrinsic geometric effects [9]. Among the emerging two-dimensional (2D) materials for polarization photodetectors, palladium diselenide (PdSe₂) has recently been brought under the spotlight [10–16]. The pentagonal intralayer Pd—Se bond networks of PdSe₂ make its symmetry (space group *Pbca* [10,11]) lower than that of hexagonal 2D materials [17,18] and endow it with anisotropic mechanical, thermal, electronic, and optical properties [14,19–21]. Moreover, PdSe₂ features extraordinarily high air stability [4,10,22], which facilitates the fabrication of PdSe₂-based devices, including field-effect transistors and photodetectors [4,11,21,22]. In contrast to the exploited transport and optoelectronic properties, the study of the electronic band structure of PdSe₂ is mainly about theoretical calculations [4,10,12,19,20,22–26] until very recently experimental approaches like angle-resolved photoemission spectroscopy (ARPES) were conducted to this material, revealing the general band structure with a strong k_z dependence

[27,28]. Currently, however, as an outstanding material for polarization photodetection, the response of its electronic band structure to light polarization has not yet been explored. Moreover, as a key parameter in the design of semiconducting devices, the calculated band gap of this compound remains controversial, and direct momentum-sensitive measurement of it is highly desired.

In this work, we reveal the orbital character of the electronic band structure of bulk PdSe₂ via polarization-dependent ARPES and density functional theory (DFT) calculations [29–37]. The conduction band minimum (CBM) is located slightly away from the high-symmetry lines near the Brillouin zone corner, and the indirect band gap is ∼0.36 eV. The polarization-dependent ARPES measurements show that the valence band (VB) top is dominated by Pd-$d_{3z^2-r^2}$ and Se-p_z orbitals, giving rise to a giant linear dichroic ratio of the top VB.

Semiconducting nature and general band structure. Bulk PdSe₂ has an orthorhombic lattice with space group *Pbca* and point group D_{2h} [10,11,38]. The crystal model with a corrugated pentagonal Pd-Se network is illustrated in Fig. 1(a). Experimental results on the electronic band structure of PdSe₂ are relatively rare compared to other 2D materials. One possible reason is that, due to the strong interlayer coupling of PdSe₂, the sample surface becomes uneven, with multiple flakes after cleavage in the ARPES chamber, as shown in Supplemental Material Fig. S1 [39]. The surface of these
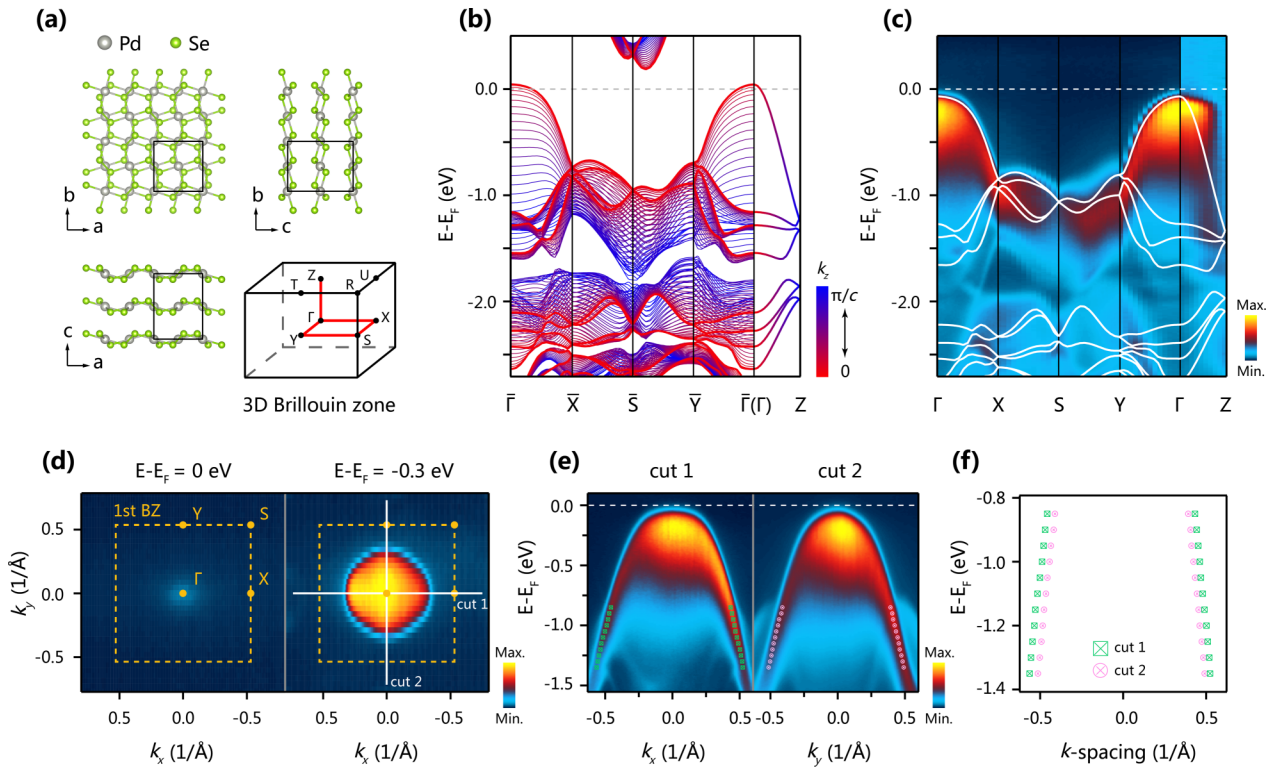
*miao@nju.edu.cn
†ynie@nju.edu.cn

FIG. 1. (a) Crystal model of $PdSe_2$ and the 3D Brillouin zone with high-symmetry points and paths. (b) Calculated band structure of bulk $PdSe_2$ along the high-symmetry path. The color scale represents a dispersion of k_z from 0 (red) to π/c (blue), and the overbars mean that the corresponding notations are only distinguished by k_x and k_y. (c) Measured band structure along the high-symmetry path. The calculated band structure with $k_z = 0$ is appended with an energy shift for comparison. (d) Constant energy maps taken at $E-E_F = 0$ and -0.3 eV. (e) VB fine-cuts measured along the $\Gamma-X$ [cut 1 in (d)] and $\Gamma-Y$ [cut 2 in (d)] directions. The peak positions of the bands away from the Fermi level are labeled by fitting the momentum distribution curves. (f) Fitted peak positions in (e).

flakes are (001) planes of the crystal but not perfectly aligned, resulting in nonuniform photoemission. To solve this problem, we performed the experiment in a synchrotron-based, spatially resolved ARPES system with a spot size of $\sim 40\ \mu$m so that the detected photoelectrons are from one single flake. First, we begin with the general electronic band structure along the high-symmetry paths as illustrated in the three-dimensional (3D) Brillouin zone of bulk $PdSe_2$ in Fig. 1(a). The calculated band structures along the high-symmetry path $\overline{\Gamma}-\overline{X}-\overline{S}-\overline{Y}-\overline{\Gamma}(\Gamma)-Z$ shown in Fig. 1(b) indicate that the VB top is located at the Γ point, where the overbars mean that the corresponding notations are only distinguished by k_x and k_y. The color scale indicates the k_z evolution from 0 (red) to π/c (blue), showing the strong k_z dependence of the energy bands, which is in agreement with previous ARPES work [27] and consistent with the strong interlayer coupling of $PdSe_2$ compared to other 2D materials, as shown in Supplemental Material Table SI [27,39–41]. The measured band structure of the as-cleaved sample along the high-symmetry path $\Gamma-X-S-Y-\Gamma-Z$ shown in Fig. 1(c) is well consistent with our calculations and previous ARPES work [27,28]. During the measurement, the incident light is linear horizontal with respect to the ground, and the used photon energy (88 eV) corresponds to the Γ plane in k_z (see Supplemental Material Fig. S2 for details [39]). The broadening of the bands and additional weak bands can be attributed to the k_z-broadening effect [42]. To trace the conduction band (CB), a constant en-

ergy map is taken at the Fermi level ($E-E_F = 0$ eV), as shown in Fig. 1(d). However, no additional feature is observed other than the weak spectral weight originating from the valence band maximum (VBM) at the Γ point, suggesting that no CB crosses the Fermi level, and the sample is a *p*-type semiconductor. Due to this semiconducting behavior of bulk $PdSe_2$, the CB of the as-cleaved sample lies above the Fermi level and cannot be observed, given the fact that only the occupied states are detectable in conventional ARPES technique. Besides, the in-plane hole effective masses of the VB along the *a*- and *b*-axes are found to be similar, which can be seen from the nearly circular hole pocket in the constant energy map 0.3 eV below the Fermi level, as shown in Fig. 1(d), and the similar peak positions of the VB along two directions shown in Figs. 1(e) and 1(f), suggesting that the reported electrical transport anisotropy of $PdSe_2$ [43] is mainly caused by other extrinsic effects like anisotropic defects distribution [44].

Band gap of bulk $PdSe_2$. To investigate the CB of $PdSe_2$ and obtain the band gap, we performed *in situ* potassium deposition to dope electrons into the sample surface, and thus shifted the energy band downward by approximately 0.56 eV with respect to the Fermi level (see Supplemental Material Fig. S3 [39]). The CB was successfully observed in the subsequent constant energy map 50 meV below the Fermi level, as illustrated in Fig. 2(a). The CBM consists of four electron pockets located slightly away from the Brillouin zone corners, which is in good agreement with our DFT results in Fig. 2(b)
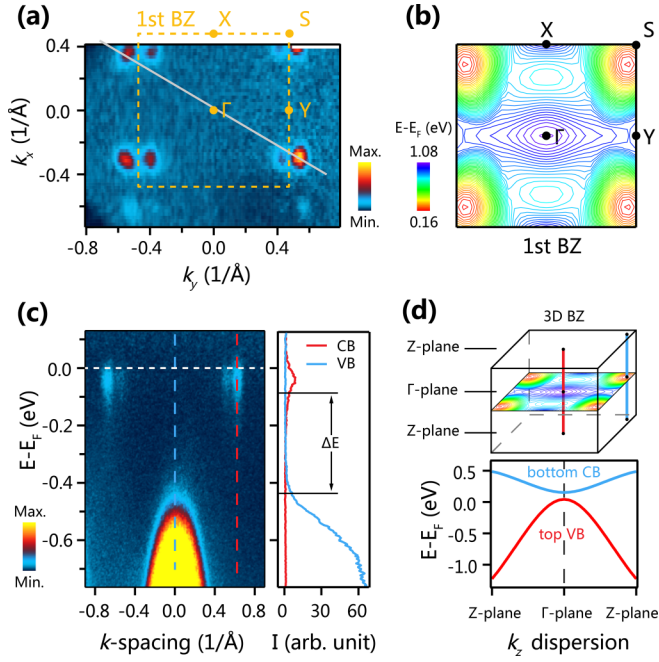
FIG. 2. (a) Measured constant energy map 50 meV below the Fermi level after potassium deposition showing the electron pockets. The Brillouin zone boundary is indicated by the orange dashed-line rectangle. (b) Calculated energy contour map showing the CBM around the Brillouin zone corner with the coordinate $(\pm 0.786\,\pi/a,\ \pm 0.929\,\pi/b)$. (c) Band dispersion taken along the gray line in (a). The CBM and VBM are observed simultaneously. Energy distribution curves of the CB (red) and VB (blue) taken from the corresponding lines are placed on the right side with an integrating width of 0.02 Å^{-1} (4 pixels). The indirect band gap ΔE is ~0.36 eV. (d) Calculated k_z dispersion of the bottom CB and the top VB. The Γ and Z planes correspond to $k_z = 0$ and π/c, respectively.

(see Supplemental Material Fig. S4 for details [39]). Moreover, we can determine the size of the band gap in bulk PdSe$_2$ by observing the CBM, which is a controversial issue both in theoretical and experimental works, as summarized in Table I [45–48]. In our experiments, the gap size is obtained by the simultaneous observation of the VBM and CBM as shown in

TABLE I. Reported gap size (E_g) of bulk PdSe$_2$.

Method	E_g (eV)	Ref.
Theory		
mBJ	0.15	[11]
mBJ	0.17	this work
PBE-GGA	0	[4]
optPBE-vdW	-0.02	[10]
optPBE-vdW	0.25	[12]
HSE06	0.57	[26]
GW	0.45	[45]
Experiment		
Optical absorption	0.5	[46]
Electrical transport	0.3	[47]
STS	0.06($\pm$0.02)	[48]

the energy-dispersive fine-cut in Fig. 2(c). The sample was azimuthally rotated so that the VBM and CBM were detected by a single cut along the gray line in Fig. 2(a). Obviously, the VBM and CBM form an indirect band gap. The energy distribution curves (EDCs) cutting through the VB and CB, indicated by the blue and red dashed lines, are drawn together and give an energy difference ΔE of approximately 0.36 eV between the VBM and CBM. Since the photon energy used here was fixed at the Γ plane, it is necessary to investigate the k_z dependence of the top VB and the bottom CB to verify if ΔE is the global minimum in the whole k-space or not. According to the DFT calculations in Fig. 2(d), both the CBM and VBM are obtained in the Γ plane, confirming that the measured ΔE of approximately 0.36 eV is indeed the band gap of bulk PdSe$_2$. As such, the indirect band gap of bulk PdSe$_2$ is experimentally demonstrated with momentum resolution for the first time.

Orbital character of the valence bands. The orbital character of the energy bands plays an important role in the periodicity doubling of the band structure and the strong interlayer coupling in PdSe$_2$ [27,28]. Although calculations are made to analyze the orbital character of PdSe$_2$, experimental investigation is limited to the unoccupied states [27]. In ARPES measurements, an incident photon source with linear polarization can distinguish states with specific symmetry relative to the plane defined by the incident light and the photoelectrons emitting toward the electron analyzer, which is called the mirror plane [49,50]. From the definition, one can notice that the mirror plane is not related to the symmetry of the sample crystal. To investigate the orbital character of PdSe$_2$, we measured the valence band structure with both p-polarized (linear horizontal with respect to the ground in our case) and s-polarized (linear vertical) light. The cuts were taken along the $\Gamma-X$ direction with a photon energy of 88 eV (Γ plane in k_z), and the geometry of the measurement is depicted in Fig. 3(a). The sample was manipulated to make the b-axis of the crystal perpendicular to the ground, and the mirror plane overlaps with the $a-c$ plane of the crystal. By switching between p- and s-polarization of the light, different bands were detected, as shown in Fig. 3(b), indicating different symmetry of the bands. To index these bands, we calculated the orbital projected density of states (DOS) and orbital projected band structures of bulk PdSe$_2$ along the $\Gamma-X$ direction. The total DOS is mainly comprised of Pd-d and Se-p orbitals, as illustrated in Fig. 3(c), which is consistent with previous work [27,28]. Moreover, by comparing the orbital projected band structures in Figs. 3(d) and 3(e) with the measured band structures in Fig. 3(b), we can understand the difference between the s- and p-polarization measurements and obtain the orbital-resolved valence band structure, which is elucidated next.

According to previous ARPES work [49,50], the s- (p-) polarization of the light would only detect electronic states whose wave functions are odd (even) with respect to the mirror plane. Considering the p and d states under an octahedral crystal field [27,28], the s-polarized light would detect p_y, d_{xy}, and d_{yz} orbitals, while the p-polarized light would detect p_x, p_z, d_{xz}, $d_{3z^2-r^2}$, and $d_{x^2-y^2}$ ones in our case. Therefore, the Pd-d_{xy}, Pd-d_{yz}, and Se-p_y orbitals can be detected by s-polarized light. However, due to the negligible spectral weight
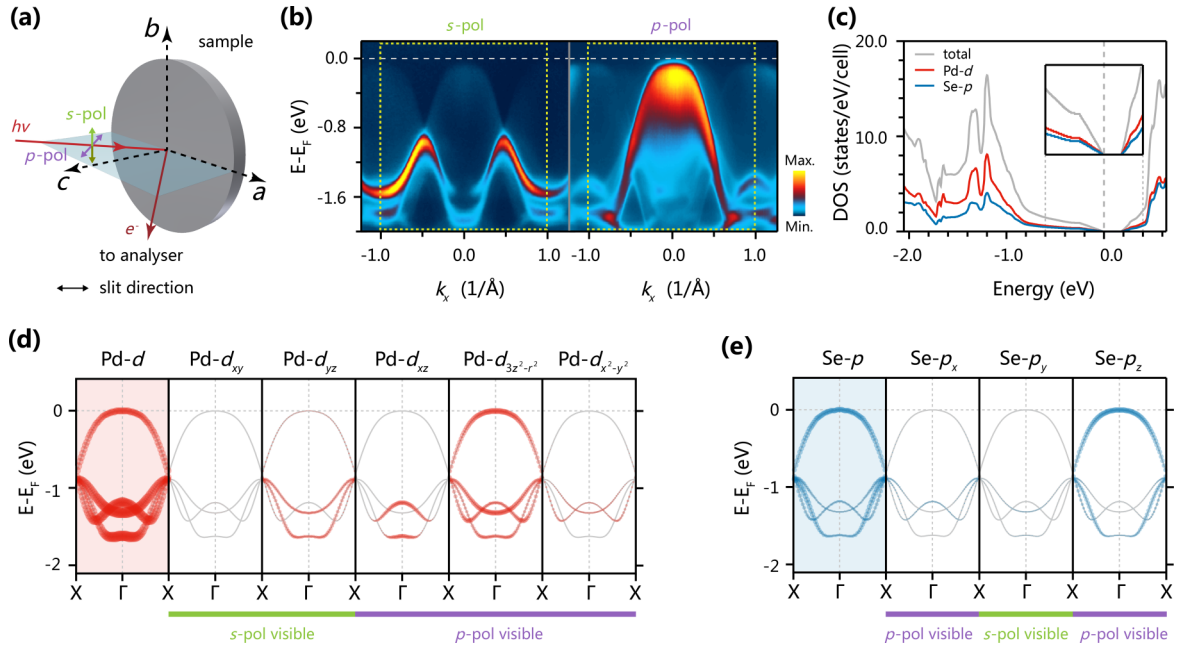
FIG. 3. Investigation of the orbital character. (a) Schematic drawing of the measuring geometry. The *b*-axis is perpendicular to the ground. The mirror plane is shown in blue color. (b) Measured VB fine structures along the $\Gamma - X$ direction with *s*- and *p*-polarized light. (c) Calculated DOS of bulk $PdSe_2$. The inset shows the vertically magnified plot near the Fermi level. (d–e) Calculated Pd-*d* and Se-*p* orbital projected valence band structures along the $\Gamma - X$ direction.

of the Pd-d_{xy} and Se-p_y orbitals near the Fermi level according to our calculations, only the Pd-d_{yz} orbital is expected to be prominently observed by the analyzer, which matches well with our experimental results shown in Fig. 3(b). For *p*-polarized light, the Pd-d_{xz} orbital was clearly observed around $k_x = \pm 1.0$ Å^{-1}, where faint features of Pd$-d_{x^2-y^2}$ + Se$-p_x$ orbitals were also detected. More importantly, the top VB is experimentally proved to be mainly comprised of Pd-$d_{3z^2-r^2}$ and Se-p_z orbitals, which is vital to understanding the atypically strong interlayer coupling in this material [27]. Lastly, the lower bands around −1.0 to −1.6 eV in the Pd-$d_{3z^2-r^2}$ and Se-p_z orbitals are absent in our *p*-polarized ARPES data, and there exists spectral weight loss of the Pd-d_{yz} band in the *s*-polarized ARPES data around $k_x = 0$ Å^{-1}. The spectral weight anomaly is possibly due to reasons such as matrix element effects, and needs further investigations. Based on the previous discussion, the orbital character of the VB in bulk $PdSe_2$ along the $\Gamma - X$ direction is experimentally resolved, and the top VB is dominated by Pd-$d_{3z^2-r^2}$ and Se-p_z orbitals.

Giant linear dichroic ratio of the valence band. The polarization-dependent ARPES results in Fig. 3(b) show that the spectral weight of the top VB is strongly dependent on the light polarization. As the linear dichroism ($I_p - I_s$) of the VB shows in Fig. 4(a), the VB top is *p*-polarization sensitive when $E - E_F$ ranges from −0.9 to 0 eV. To quantify the polarization sensitivity, we integrated the EDCs of the VB under *s*- and *p*-polarized light within the region denoted by the yellow rectangles, as shown in Fig. 3(b), and plotted the linear dichroic ratio I_p/I_s and the normalized linear dichroism ($I_p - I_s$)/($I_p + I_s$) as functions of $E - E_F$, as illustrated in Figs. 4(b) and 4(c). When $E - E_F$ ranges from − 0.9 to 0 eV, the ARPES spectral weight under *p*-polarized light is obviously

larger than that from *s*-polarized light, leading to a giant linear dichroic ratio of ∼10 (corresponds to a normalized linear dichroism of 0.82). To the best of our knowledge, this is the largest linear dichroic ratio among the polarization-dependent ARPES works [51–55]. More importantly, this giant linear dichroic ratio quantitatively demonstrates that the VBM is dominated by the out-of-plane Pd-$d_{3z^2-r^2}$ and Se-p_z orbitals, which is contrast to the in-plane dominated states at the CBM revealed by previous X-ray absorption spectroscopy linear
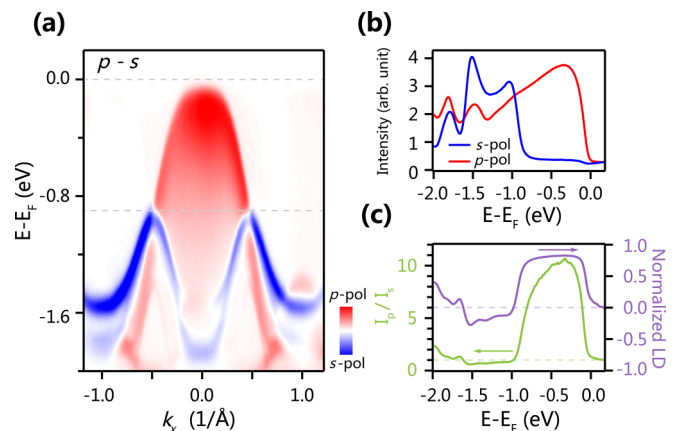

FIG. 4. Giant linear dichroic ratio in $PdSe_2$. (a) Linear dichroism ($I_p - I_s$) of the VB measured along the $\Gamma - X$ direction. I_p (I_s) corresponds to the spectral weight under *p*- (*s*-)polarized light. (b) Integrated EDCs of the VB with *s*- and *p*-polarized light. The data were integrated within the region denoted by the yellow rectangles as shown in Fig. 3(b). (c) Linear dichroic ratio (I_p/I_s) and normalized linear dichroism [($I_p - I_s$)/($I_p + I_s$)] of the VB from − 2.0 to 0.2 eV calculated from (b).

dichroism (XLD) measurements [27]. Our results provide a complete picture of the orbital character near the Fermi level together with the previous XLD results, and illustrate the huge orbital-induced anisotropy in this material. Based on this point, we propose PdSe$_2$ as a novel orbital-engineered material for optical applications. For example, the selection rule of electric dipole transition is closely related to the light polarization and the orbital character of the energy bands [56], so PdSe$_2$ with orbital-engineered band structures could interact differently with different light polarizations and incident angles [57]. In addition, compounds like PdS$_2$ may also exhibit similar giant orbital anisotropy, which is worth exploring in the future.

Conclusions. The electronic band structure of bulk PdSe$_2$ is revealed by ARPES and DFT calculations. The VBM is observed at the Brillouin zone center, and the CBM is detected near the Brillouin zone corner by potassium deposition, forming an indirect band gap of $\sim$0.36 eV. Moreover, the orbital character analysis shows that the top VB is dominated by Pd-$d_{3z^2-r^2}$ and Se-p_z orbitals, and this gives rise to a giant linear dichroic ratio of $\sim$10. Our work elucidates the semiconducting nature of PdSe$_2$ and proposes PdSe$_2$ as a novel, intrinsically orbital-engineered material with giant anisotropy for polarization-related optical applications.

[1] G. Cincotti, IEEE J. Quantum Elect. **39**, 1645 (2003).

[2] A. Rubin Noah, G. D'Aversa, P. Chevalier, Z. Shi, T. Chen Wei, and F. Capasso, Science **365**, eaax1839 (2019).

[3] T.-H. Chiou, S. Kleinlogel, T. Cronin, R. Caldwell, B. Loeffler, A. Siddiqi, A. Goldizen, and J. Marshall, Curr. Biol. **18**, 429 (2008).

[4] D. Wu, J. Guo, J. Du, C. Xia, L. Zeng, Y. Tian, Z. Shi, Y. Tian, X. J. Li, Y. H. Tsang, and J. Jie, ACS Nano **13**, 9907 (2019).

[5] L. Li, P. Gong, D. Sheng, S. Wang, W. Wang, X. Zhu, X. Shi, F. Wang, W. Han, S. Yang, K. Liu, H. Li, and T. Zhai, Adv. Mater. **30**, 1804541 (2018).

[6] L. Li, W. Wang, P. Gong, X. Zhu, B. Deng, X. Shi, G. Gao, H. Li, and T. Zhai, Adv. Mater. **30**, 1706771 (2018).

[7] Y. Wang *et al.*, Adv. Mater. **32**, 2005037 (2020).

[8] R. Chai, Y. Chen, M. Zhong, H. Yang, F. Yan, M. Peng, Y. Sun, K. Wang, Z. Wei, W. Hu, Q. Liu, Z. Lou, and G. Shen, J. Mater. Chem. C **8**, 6388 (2020).

[9] H. Yuan, X. Liu, F. Afshinmanesh, W. Li, G. Xu, J. Sun, B. Lian, A. G. Curto, G. Ye, Y. Hikita, Z. Shen, S.-C. Zhang, X. Chen, M. Brongersma, H. Y. Hwang, and Y. Cui, Nat. Nanotechnol. **10**, 707 (2015).

[10] A. D. Oyedele, S. Yang, L. Liang, A. A. Puretzky, K. Wang, J. Zhang, P. Yu, P. R. Pudasaini, A. W. Ghosh, Z. Liu, C. M. Rouleau, B. G. Sumpter, M. F. Chisholm, W. Zhou, P. D. Rack, D. B. Geohegan, and K. Xiao, J. Am. Chem. Soc. **139**, 14090 (2017).

[11] W. L. Chow, P. Yu, F. Liu, J. Hong, X. Wang, Q. Zeng, C.-H. Hsu, C. Zhu, J. Zhou, X. Wang, J. Xia, J. Yan, Y. Chen, D. Wu, T. Yu, Z. Shen, H. Lin, C. Jin, B. K. Tay, and Z. Liu, Adv. Mater. **29**, 1602969 (2017).

[12] M. A. ElGhazali, P. G. Naumov, H. Mirhosseini, V. Süß, L. Müchler, W. Schnelle, C. Felser, and S. A. Medvedev, Phys. Rev. B **96**, 060509(R) (2017).

[13] S. Y. Akinola, D. Oyedele, T. Feng, A. V. Haglund, Y. Gu, A. A. Puretzky, D. Briggs, C. M. Rouleau, M. F. Chisholm, R. R. Unocic, D. Mandrus, H. M. Meyer III, S. T. Pantelides, D. B. Geohegan, and K. Xiao, J. Am. Chem. Soc. **141**, 8928 (2019).

[14] W. Luo, A. D. Oyedele, Y. Gu, T. Li, X. Wang, A. V. Haglund, D. Mandrus, A. A. Puretzky, K. Xiao, L. Liang, and X. Ling, Adv. Func. Mater. **30**, 2003215 (2020).

[15] M. Sun, J.-P. Chou, L. Shi, J. Gao, A. Hu, W. Tang, and G. Zhang, ACS Omega **3**, 5971 (2018).

[16] L. Jia, J. Wu, T. Yang, B. Jia, and D. J. Moss, ACS Appl. Nano Mater. **3**, 6876 (2020).

[17] T. Rohwer, S. Hellmann, M. Wiesenmayer, C. Sohrt, A. Stange, B. Slomski, A. Carr, Y. Liu, L. M. Avila, M. Kalläne, S. Mathias, L. Kipp, K. Rossnagel, and M. Bauer, Nature (London) **471**, 490 (2011).

[18] J. M. Riley, W. Meevasana, L. Bawden, M. Asakawa, T. Takayama, T. Eknapakul, T. K. Kim, M. Hoesch, S.-K. Mo, H. Takagi, T. Sasagawa, M. S. Bahramy, and P. D. C. King, Nat. Nanotechnol. **10**, 1043 (2015).

[19] D. Qin, P. Yan, G. Ding, X. Ge, H. Song, and G. Gao, Sci. Rep. **8**, 2764 (2018).

[20] J. Sun, H. Shi, T. Siegrist, and D. J. Singh, Appl. Phys. Lett. **107**, 153902 (2015).

[21] Q. Liang, Q. Wang, Q. Zhang, J. Wei, S. X. Lim, R. Zhu, J. Hu, W. Wei, C. Lee, C. Sow, W. Zhang, and A. T. S. Wee, Adv. Mater. **31**, 1807609 (2019).

[22] M. Long, Y. Wang, P. Wang, X. Zhou, H. Xia, C. Luo, S. Huang, G. Zhang, H. Yan, Z. Fan, X. Wu, X. Chen, W. Lu, and W. Hu, ACS Nano **13**, 2511 (2019).

[23] X. Liu, H. Zhou, B. Yang, Y. Qu, and M. Zhao, Sci. Rep. **7**, 39995 (2017).

[24] A. V. Kuklin and H. Ågren, Phys. Rev. B **99**, 245114 (2019).

[25] L.-H. Zeng, D. Wu, S.-H. Lin, C. Xie, H.-Y. Yuan, W. Lu, S. P. Lau, Y. Chai, L.-B. Luo, Z.-J. Li, and Y. H. Tsang, Adv. Func. Mater. **29**, 1806878 (2019).

[26] W. Lei, B. Cai, H. Zhou, G. Heymann, X. Tang, S. Zhang, and X. Ming, Nanoscale **11**, 12317 (2019).

[27] J. H. Ryu, J.-G. Kim, B. Kim, K. Kim, S. Kim, J.-H. Park, B.-G. Park, Y. Kim, K.-T. Ko, and K. Lee, Small **18**, 2106053 (2022).

[28] M. Cattelan, C. J. Sayers, D. Wolverson, and E. Carpene, 2D Mater. **8**, 045036 (2021).

[29] G. Kresse and J. Furthmüller, Comput. Mater. Sci. **6**, 15 (1996).

[30] G. Kresse and J. Furthmüller, Phys. Rev. B **54**, 11169 (1996).

[31] P. E. Blöchl, Phys. Rev. B **50**, 17953 (1994).

[32] G. Kresse and D. Joubert, Phys. Rev. B **59**, 1758 (1999).

[33] J. P. Perdew, A. Ruzsinszky, G. I. Csonka, O. A. Vydrov, G. E. Scuseria, L. A. Constantin, X. Zhou, and K. Burke, Phys. Rev. Lett. **100**, 136406 (2008).

[34] D. J. Singh and L. Nordstrom, *Planewaves, Pseudopotentials and the LAPW Method*, 2nd ed. (Springer, Berlin, 2006).

[35] K. Schwarz, P. Blaha, and G. K. H. Madsen, Comput. Phys. Commun. **147**, 71 (2002).

[36] A. D. Becke and E. R. Johnson, J. Chem. Phys. **124**, 221101 (2006).

[37] F. Tran and P. Blaha, Phys. Rev. Lett. **102**, 226401 (2009).

[38] C. Soulard, X. Rocquefelte, P. E. Petit, M. Evain, S. Jobic, J. P. Itie, P. Munsch, H. J. Koo, and M. H. Whangbo, Inorg. Chem. **43**, 1943 (2004).

[39] See Supplemental Material at http://link.aps.org/supplemental/10.1103/PhysRevB.106.L121110 for method and additional results.

[40] L. X. Benedict, N. G. Chopra, M. L. Cohen, S. G. Louie, and V. H. Crespi, Chem. Phys. Lett. **286**, 490 (1998).

[41] Y. Wang, Y. Li, and Z. Chen, J. Mater. Chem. C **3**, 9603 (2015).

[42] C. Chen *et al.*, Matter **3**, 2055 (2020).

[43] L. Pi, C. Hu, W. Shen, L. Li, P. Luo, X. Hu, P. Chen, D. Li, Z. Li, X. Zhou, and T. Zhai, Adv. Func. Mater. **31**, 2006774 (2021).

[44] X. Liu *et al.*, Phys. Rev. Mater. **5**, L041001 (2021).

[45] H.-G. Kim and H. J. Choi, Phys. Rev. B **103**, 165419 (2021).

[46] G. Zhang, M. Amani, A. Chaturvedi, C. Tan, J. Bullock, X. Song, H. Kim, D.-H. Lien, M. C. Scott, H. Zhang, and A. Javey, Appl. Phys. Lett. **114**, 253102 (2019).

[47] W. Nishiyama, T. Nishimura, K. Ueno, T. Taniguchi, K. Watanabe, and K. Nagashio, Adv. Func. Mater. **32**, 2108061 (2021).

[48] G. D. Nguyen, L. Liang, Q. Zou, M. Fu, A. D. Oyedele, B. G. Sumpter, Z. Liu, Z. Gai, K. Xiao, and A.-P. Li, Phys. Rev. Lett. **121**, 086101 (2018).

[49] R. Bistritzer, G. Khalsa, and A. H. MacDonald, Phys. Rev. B **83**, 115114 (2011).

[50] A. Damascelli, Z. Hussain, and Z.-X. Shen, Rev. Mod. Phys. **75**, 473 (2003).

[51] B. K. Choi, S. Ulstrup, S. M. Gunasekera, J. Kim, S. Y. Lim, L. Moreschini, J. S. Oh, S.-H. Chun, C. Jozwiak, A. Bostwick, E. Rotenberg, H. Cheong, I.-W. Lyo, M. Mucha-Kruczynski, and Y. J. Chang, ACS Nano **14**, 7880 (2020).

[52] T. Hirahara, T. Shirai, T. Hajiri, M. Matsunami, K. Tanaka, S. Kimura, S. Hasegawa, and K. Kobayashi, Phys. Rev. Lett. **115**, 106803 (2015).

[53] T. Sugimoto, D. Ootsuki, C. Morice, E. Artacho, S. S. Saxena, E. F. Schwier, M. Zheng, Y. Kojima, H. Iwasawa, K. Shimada, M. Arita, H. Namatame, M. Taniguchi, M. Takahashi, N. L. Saini, T. Asano, R. Higashinaka, T. D. Matsuda, Y. Aoki, and T. Mizokawa, Phys. Rev. B **92**, 041113(R) (2015).

[54] S. Soltani, S. Cho, H. Ryu, G. Han, B. Kim, D. Song, T. K. Kim, M. Hoesch, and C. Kim, Phys. Rev. B **95**, 125103 (2017).

[55] E. Lee, D. H. Kim, J. D. Denlinger, J. Kim, K. Kim, B. I. Min, B. H. Min, Y. S. Kwon, and J. S. Kang, Phys. Rev. B **91**, 125137 (2015).

[56] G. Wang, C. Robert, M. M. Glazov, F. Cadiz, E. Courtade, T. Amand, D. Lagarde, T. Taniguchi, K. Watanabe, B. Urbaszek, and X. Marie, Phys. Rev. Lett. **119**, 047401 (2017).

[57] C. Fang, M. Xu, J. Ma, J. Wang, L. Jin, M. Xu, and D. Li, Nano Lett. **20**, 2339 (2020).